Aalborg Universitet

Stabilization of a ROV in Three-dimensional Space Using an Underwater Acoustic Positioning System

Pedersen, Simon; Liniger, Jesper; Sørensen, Fredrik Fogh; Schmidt, Kenneth; von Benzon, Malte Severin Rosencrone; Klemmensen, Sigurd Stoltenberg

Stabilization of a ROV in Three-dimensional Space Using an Underwater Acoustic Positioning System

Simon Pedersen [*,★] Jesper Liniger [*] Fredrik F. Sørensen [*]
Kenneth Schmidt [*] Malte von Benzon [*]
Sigurd S. Klemmensen [*]

[*] *Department of Energy Technology, Aalborg University, Niels Bohrs Vej 8, 6700 Esbjerg, Denmark.*

Abstract: In subsea applications there are an increasing demand for Remotely Operated Vehicles (ROV's). This study examines a BlueROV2 inspection ROV prototype for autonomous operation in three-dimensional space. This study describes the ROV modelling, identification, control development and closed-loop simulations and experiments. The main transmitter applied for the navigation is an Underwater Acoustic Positioning System (UAPS) which acts as an underwater GPS unit. The transmitter introduces a dominant output time delay which is handled by a smith predictor. The results show that the smith predictor does not handle the time delay well, probably because the time delay is time-variant. Online identification of the time delay is proposed as a potential solution for minimizing the impact of the time delay variations over time.

Keywords: Time delay, mathematical modeling, subsea control, ROV, offshore robotics

1. INTRODUCTION

Underwater robots are used in an increasing amount of tasks, such as mapping, surveillance, welding, inspections and assembly (Mai et al. (2016); Wynn et al. (2014)). The offshore industry is the biggest user of Remotely Operated Vehicles (ROVs) and Autonomous Underwater Vehicles (AUVs); primarily because of a decrease in operational cost over the last few years, see Reid (2013); Brun (2014); Marine Technology Society (2017). Globally, most industrial ROV operations are manually controlled, with neither automatic control functions nor other autonomous capabilities Schjølberg and Utne (2015). However, automation has proven to decrease both the time and cost of operation Tena (2011). One limitation of subsea operations is determining the positioning of the ROV, as the relative position are restricted by the transmitters available (Fossen (2011)). Typically, these transmitters are either gyroscopes or accelerometers with drifting, noisy or deviating measurement properties, which often result in imprecise and unreliable measurement signals (Mai et al. (2017); Arnesen et al. (2017); Pedersen et al. (2018)). Besides, there exist a lack of absolute positioning transmitters due to the fact that GPS signal does not operate subsea.

This paper will examine a BlueROV2, which is a ROV prototype developed for minor offshore inspection tasks. The described work's objective is to stabilize the three-dimensional position of the ROV using an underwater acoustic positioning transmitter where there exist an dominant time delay in the measured output. The acoustic transmitter operates as an underwater GPS. The positioning transmitter will be investigated as an alternative to the commonly applied transmitters for real-time feedback control of ROVs. First, a model of the ROV is described and identified, then a controller is developed using a LQRI full-state feedback controller with a smith predictor on the linearized model. The controller is both evaluated in closed-loop simulations and experiments in a water basin to demonstrate the closed-loop performance of the system.

2. PLATFORM

The ROV used in the project is provided by the company Blue Robotics Inc. and is a BlueROV2, see figure 1. The ROV is powered by a battery and is controlled from the surface by computer through a tether. The ROV moves around using six thrusters which are paired. The embedded software do not allow for control of each thruster individually, but are preprogrammed to actuate the ROV in specific predetermined directions. Thus, the ROV is directly able to sway, heave, surge, roll and yaw as seen on figure 1 To monitor the ROV the onboard sensors in the IMU are used as feedback. The IMU provides the ROVs depth and orientation. To determine the 3-dimensional position in space an underwater positioning system is installed on the ROV. An Underwater Acoustic Positioning System (UAPS) developed by WaterLinked is used. The UAPS transmits acoustic waves from the ROV to several receivers on the water surface that calculate the ROV's position based on trilateration distance calculations (Joaqun Aparicio and lvarez (2016)). In this configuration the UAPS uses Short Baseline (SBL) with four transducers which is lowered into the water, and send signals back to a ground station, which is above water level.

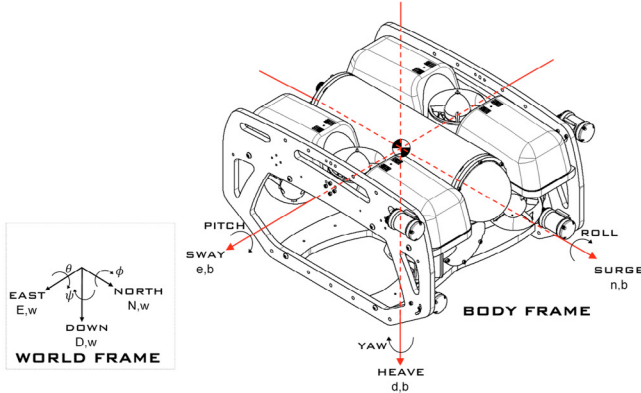★ Corresponding author. E-mail: spe@et.aau.dk.

Fig. 1. The ROV placed in the two respective coordinate systems; the body and the world frame.
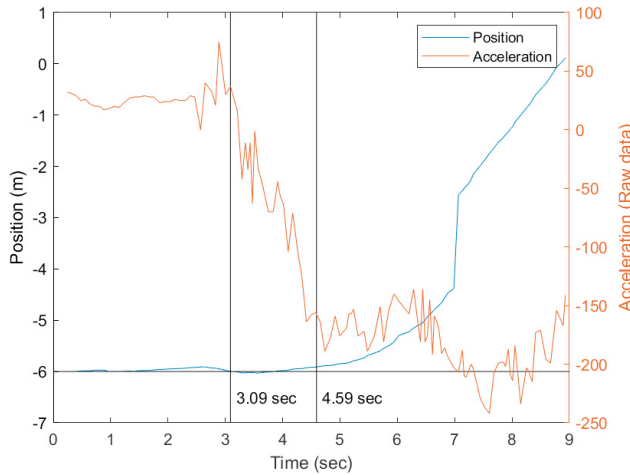

Fig. 2. The accelerometer and UAPS data in the x-coordinate. Notice that the figure only illustrates that time at which the transmitters detects the motion chance and that the units from the two transmitters are not comparable.

In figure 2 the UAPS data is logged together with the acceleration data as a thruster step input is given to the surge motion (x-coordinate). The step input is given at 3 seconds. Although the accelerometer has the most noise, it is clear that it reacts immediately to the motion change. Hence, there is a time delay in the UAPS communication to the real-time operating computer. By doing several experiments the time delay, τ, is estimated to be $\tau = 2.05 \pm 0.55s$.

3. MODEL

The model description is divided into three subsystems: The ROV frame, the thruster forces and the damping forces.

3.1 Dynamic model

The dynamic behavior of the ROV is based on the Lagrangian relationship:

$$L = T - V \tag{1}$$

where V is a function of the generalized position vector that describes the potential energy of the ROV, and T is the kinetic energy of the moving ROV, not considering the fluid, but only rotation and translation, such that the vector form is

$$T = \frac{1}{2}v^T M v \tag{2}$$

where M is the mass matrix and v is the generalized velocity vector. For the rotational motion v is replaced by the angular velocity and m is replaced by the mass moment of inertia. The potential energy of the system is given solely from the buoyancy force acting on the ROV, when the ROV is orientated of its stable point in either pitch or roll it creates a force and a moment moving the ROV back into its stable position. At its stable position the center of the buoyancy (COB) is located straight above the center of mass (COM) as shown in figure 4. Meaning that the angles θ and ϕ are zero. The buoyancy force which is acting on the ROV creates a torque with the distance from the COB to the resting position. This distance can be found since the distance between the COM and the COB is fixed. The distance in the D,w direction, between the COM and COB can be found by transforming the rotation matrix, R_f, and converting the L_{GB} from body to world frame. As the L_{GB} is described for body frame, the D component of the vector for the length between COM and COB is given by

$$\begin{pmatrix} 0 \\ 0 \\ L_{GB,D,w} \end{pmatrix} = \begin{pmatrix} 0 \\ 0 \\ L_{GB,d,b} \end{pmatrix} \cdot \mathbf{R}_f \tag{3}$$

As the ROV is assumed to be neutrally buoyant the total potential energy, V, is

$$V = -L_{GB,D,\omega} F_b \tag{4}$$

where F_b is the force due to buoyancy of the ROV, $F_b = \rho g v$, with ρ being the density of water and, g the gravitational acceleration and v the volume of the ROV. $L_{GB,D,\omega}$ can be obtained from

$$-L_{GB,D,b} = -L_{GB,d,b} cos(\theta) cos(\phi) \tag{5}$$

Now the Lagrangian can be obtained:

$$L = \frac{1}{2} \cdot \mathbf{v}_w^T \cdot \mathbf{M}_{rb} \cdot \mathbf{v}_w - l_{b\theta} \cdot Fb - l_{b\phi} \cdot Fb \tag{6}$$

which can be included in the Euler-Lagrange equation,

$$\frac{d}{dt}\left(\frac{\delta L}{\delta \mathbf{v}_w}\right) - \frac{\delta L}{\delta \mathbf{p}_w} = \mathbf{T}_f \cdot \mathbf{F}_b \tag{7}$$

The first term in equation 7 is

$$\frac{d}{dt}\left(\frac{\delta L}{\delta \mathbf{v}_w}\right) = \begin{pmatrix} \mathbf{M}_{RB} & 0 \\ 0 & \mathbf{I}_O \end{pmatrix} \cdot \mathbf{a}_w \tag{8}$$

The second term is the restoring forces and are given as,

$$\frac{\delta L}{\delta \mathbf{p}_w} = \begin{pmatrix} 0 \\ \mathbf{G} \end{pmatrix} \cdot \tag{9}$$

Here, $\mathbf{G}$ represents the restoring forces (Fossen (1994)). $\mathbf{T}_f$ is a transformation matrix, which transforms the drag forces to torques by considering the distance from the thruster to the COM, this is $\mathbf{L}_s$ and $\mathbf{L}_r$. It also transforms the body fixed translational forces to world frame by applying a rotation matrix $\mathbf{R}_f$.

$$\mathbf{T}_f = \begin{pmatrix} \mathbf{R}_f & \mathbf{0} \\ \mathbf{L}_s & \mathbf{L}_r \end{pmatrix} \tag{10}$$
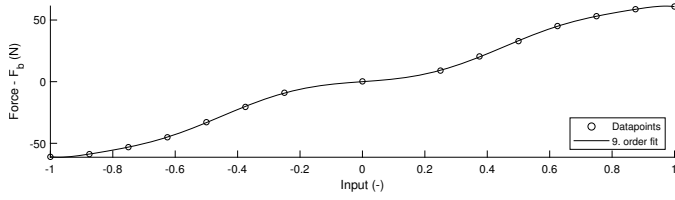
Fig. 3. Shows force provided by 2 thruster with input from -100% to 100 %. A 9th order polynomial is applied to obtained an acceptable model accuracy.

3.2 Thruster model

The thruster percentage to force must be modeled to find the correct actuator forces acting on the ROV. The thruster expression is obtained from Wang and Clark (2006):

$$F_{thrust} = \rho D^4 \left(\alpha_1 + \frac{\alpha_2 \cdot u_a}{nD} \right) \cdot \eta|\eta| \qquad (11)$$

where $\alpha_{1,2}$ are the thruster coefficients describing the efficiency of the propeller, D is diameter, u_a is the ambient water speed, F_{thrust} is the thrust of the propeller and η is the propeller rate. The coefficients in the thruster model are identified by connecting a newton meter to the ROV in water and gradually increasing the dedicated heave thrusters by 10 % in step size until reaching steady-state. The results are plotted in figure 3 where the modelled is fitted to a static 9th order polynomial. The obtained coefficients are used for all directions as it is assumed that the ROV has no geometry that will affect the flow from the thrusters unevenly. Motion around the axes, known as rotations, is possible through the thrusters applying torque to the ROV. The length from the thrusters to the center of gravity need to befound to determine the size of this torque, see figure 4 and 5.
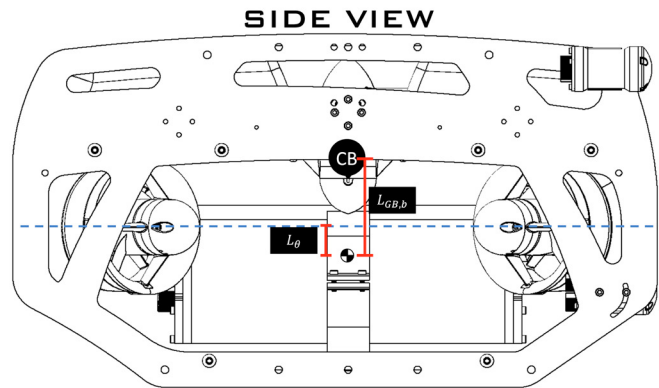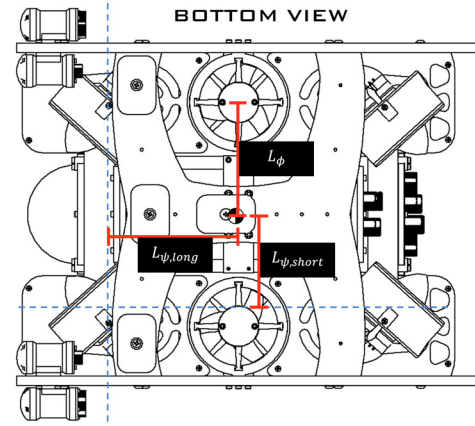

Fig. 5. The ROV with the lengths between COM and centerlines of thrusters. Blue dotted line is the centerline of thrusters

Hence, the pitch moment, $M_{\theta,n}$, is a function of the surge thruster force: $M_{\theta,n} = F_{n,b} \cdot L_\theta$, the moment caused by the roll thrusters can be described by $M_\phi = F_{\phi,b} \cdot L_\phi$, the roll moment for sway can be described by $M_{\phi,e} = F_{e,b} \cdot L_\theta$ where the length is the same as for the pitch. The yaw motion is effected by all four horizontal thrusters: $M_\psi = F_{\psi,b} \cdot L_{\psi,long} + F_{\psi,b} \cdot L_{\psi,short}$.

3.3 Damping forces

The damping forces derive from two sources, the drag and the added mass. The added mass is neglected in this project as it only is resisting movement during accelerations, and therefore, compared to the drag force it is thought to be insignificant at smaller accelerations. The general drag force for one direction is given by

$$f_{drag} = \frac{1}{2} \cdot c_d \cdot \rho \cdot A \cdot v^2 \qquad (12)$$

where c_d is the drag coefficient and A is the cross sectional area perpendicular to the flow. c_d is a combination of skin friction drag and pressure drag, but can be assumed to be constant at Reynolds numbers between $10^3 - 10^5$ (Cengel (2012)), which is assumed to be present in this study.

Fig. 4. The ROV with the lengths between COM and centerlines of thrusters. Blue dotted line is the centerline of thrusters
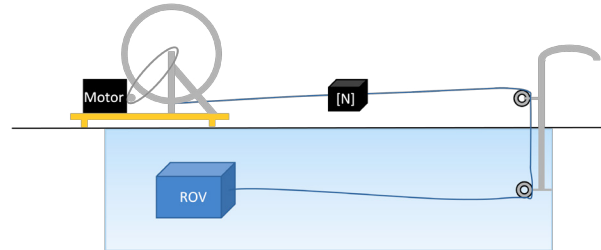

Fig. 6. Illustration of the test setup for determination of drag forces.

Figure 6 illustrates the test setup used to identify the C_d coefficients. To find the force-velocity relations, the ROV

is dragged through the water with constant velocity by a motor and the force required to do so is measured with a Newton meter. This procedure is carried out for surge and sway, but as the distance for the vertical movement (heave) is limited by the test facility, a different test is performed where weight is added to the ROV and the downwards acting force is measured. For the rotational movements of the ROV, described as roll, pitch and yaw, a lesser accurate method is used, as these movements do not influence the ROV as much. For yaw and roll, the maximum angular velocity is found together with the angular velocity at 50 % thrust. This provides three points as the drag torque should always go through 0. The pitch is identified by applying equation (11) to determine C_d based on a known velocity. It is assumed that the drag for the front is equal the back, and drag for the top is equal the bottom. Then, the drag torque for pitch can be determined as an expression for linear drag on a rotational movement, such that

$$M_{d\theta,b} =$$

$$2 \cdot \int_0^{\frac{L_{side}}{2}} \frac{1}{2} \cdot \rho \cdot (\omega_{\theta,b} \cdot r_1)^2 \cdot (r_1 \cdot L_{for}) \cdot Cd_{top} \ dr_1 +$$

$$2 \cdot \int_0^{\frac{h}{2}} \frac{1}{2} \cdot \rho \cdot (\omega_{\theta,b} \cdot r_2)^2 \cdot (r_2 \cdot L_{for}) \cdot Cd_{for} \ dr_2$$

$$(13)$$

3.4 The complete model

After the model was identified it was validation based on a variety of experiments. The error distribution with subject to thruster actuation showed that the model overall is sufficiently accurate for model-based control applications. The combined model description can be expressed by equation (14).

$$\begin{pmatrix} \mathbf{M}_{RB} & \mathbf{0} \\ \mathbf{0} & \mathbf{I}_O \end{pmatrix} \cdot \mathbf{a}_w - \begin{pmatrix} \mathbf{0} \\ \mathbf{G} \end{pmatrix} = \mathbf{f}_{b,b} \cdot \begin{pmatrix} \mathbf{R}_f & \mathbf{0} \\ \mathbf{L}_s & \mathbf{L}_r \end{pmatrix} - \mathbf{f}_{d,b} \cdot \begin{pmatrix} \mathbf{R}_f & \mathbf{0} \\ \mathbf{0} & \mathbf{I}_3 \end{pmatrix}$$

$$(14)$$

A table with all model parameters and dimensions is seen in the table 1.

Table 1. Table of all parameters

Description	Symbol	Value	Unit
Volume	v	0.011167	m^3
Length from COM to COB	$L_{GB,b}$	0.028	m
Length from COM to pitch thruster	L_ϕ	0.005	m
Length from COM to roll thruster	L_θ	0.111	m
Short length from G to yaw thruster	$L_{\psi,short}$	0.148	m
Long length from G to yaw thruster	$L_{\psi,long}$	0.089	m
Height of ROV	h	0.254	m
Length of side	L_{side}	0.457	m
Length of front	L_{front}	0.338	m
Drag coefficient for front and back	Cd_{for}	1.6	-
Drag coefficient for top and bottom	Cd_{top}	1.48	-
Mass of ROV	m	11.167	kg
MOI around x axis	I_ϕ	0.2	$kg \cdot m^2$
MOI around y axis	I_θ	0.243	$kg \cdot m^2$
MOI around z axis	I_ψ	0.239	$kg \cdot m^2$

4. CONTROL DEVELOPMENT

This section describes the control development which consists of a Linearquadratic regulator with integral action (LQRI) including a Smith predictor.

4.1 Linearization and open-loop analysis

The model is linearized using Taylor expansion to obtain the state-space Jacobians. The linearized model is compared to the non-linear model, and the comparison shows that the linear model deviates somewhat from the non-linear model. One of the experiments is shown in figure 7 where a unity input step is applied to the surge thrusters. As this motion also impacts the pitching, the pitch output is also plotted. The respective transient responses are almost identical, while a larger deviation exist at steady-state. This can be explained by the thruster operating far from the linearization point.
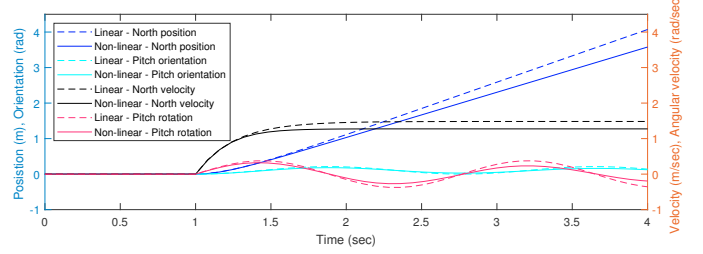

Fig. 7. This figure shows the simulated linear and non-linear models when a unit step is applied to the surging thrusters.

The obtained linearized state-space model consists of all positions, orientations, velocities and angular velocities are added as states; which results in a total of 12 states. Although the velocities are not directly measured, they are simply derivatives of the 6 measured outputs, resulting in 12 outputs. The model is both fully controllable and observable as the observability and controllability matrices have full rank. The model is marginally stable as the poles related to the positions are located at the origin of the s-plane.

4.2 Linear quadratic regulator with integral action

The LQR controller is a full-state feedback optimal control method which finds the minimimum solution to a defined cost function. LQR is unconstrained which means it is not possible to define saturation limits directly into the method. The cost function penalizes both the inputs and states of the system to find a controller gain, $\mathbf{K}$, such that $\mathbf{u} = -\mathbf{Kx}$. The cost function, $\mathbf{J}$, is defined as a time integration of the two respective weighted terms, such that

$$\mathbf{J(t)} = \int_0^\infty \left(\mathbf{x(t)}^T \cdot \mathbf{Q} \cdot \mathbf{x(t)} + \mathbf{u(t)}^T \cdot \mathbf{R} \cdot \mathbf{u(t)} \right) dt$$

$$(15)$$

where $\mathbf{J(u)}$ is the cost function, $\mathbf{x}$ is the states, $\mathbf{u}$ is the inputs, $\mathbf{Q}$ is a 16x16 semi-positive definite matrix which weighs the states and $\mathbf{R}$ is a 5x5 is a positive definite matrix whitch weighs the inputs.

To eliminate steady-state error for any output an integral term is introduced, such that the updated system can be expressed as

$$\begin{pmatrix} \dot{\mathbf{x}}_i \\ \dot{\mathbf{x}}_s \end{pmatrix} = \begin{pmatrix} \mathbf{0} & \mathbf{C} \\ \mathbf{0} & \mathbf{A} \end{pmatrix} \cdot \begin{pmatrix} \mathbf{x}_i \\ \mathbf{x} \end{pmatrix} + \begin{pmatrix} \mathbf{0} \\ \mathbf{B} \end{pmatrix} \cdot \mathbf{u} - \mathbf{B}_r \cdot \mathbf{ref} \quad (16)$$

where $\mathbf{u} = -\mathbf{K_a x}$, $\mathbf{K_a} = [\mathbf{K_i} \ \mathbf{K}]$ and $\mathbf{B_r}$ (16x4) is a matrix which scales the reference to be the same size as the other
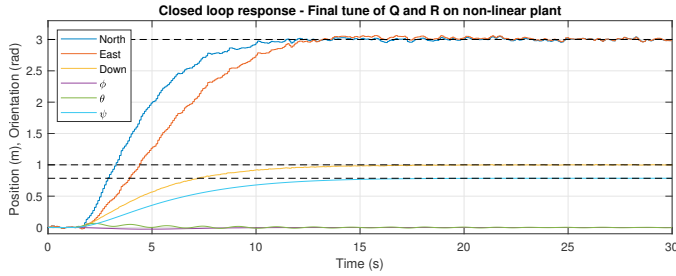
Fig. 8. Output response of a reference change of 3 m in n_w and e_w, 1 m in d_w and a change in orientation of $\frac{\pi}{4}$ in ψ_w, with the final LQRI controller simulated with the non-linear model.

Fig. 10. Result for steady position controller with the obtained controller, the red dot is the initial position

components in the system. The new **A** and **B** matrices are used, such that **Q** (16x16) weights 16 states and **R** (5x5) still weights 5 inputs.

Bryson's rule is applied for the **Q** and **R** matrices similar to Mai et al. (2017). By normalizing the states' and inputs' maximum values this method ensures that all are weighted equally from the beginning. The **Q** and **R** matrices are then manually tuned further based on non-linear model simulations, which leads to a decrease in the integral terms in order to minimize the overshooting. In this tuning process, the pitch penalty is also decreased to allow a more aggressive surge motion. Moreover, integral anti-windup is added to all integral terms to avoid the integral term to accumulate when the ROV is far from the reference point and the actuators are saturated. The final non-linear closed-loop simulation of the theoretically tuned output responses is seen on figure 8. The control objective was to reduce the overshooting to a minimum while keeping an acceptable settling time. Thus, based on the simulations the controller was found acceptable for fulfilling the objectives.

4.3 Smith predictor

The time delay from the UAPS sensor is addressed by included a smith predictor to the control scheme. A Smith predictor predicts the positions of the the ROV and corrects potential model deviations by subtracting time delayed model outputs from the corresponding measured values. Figure 9 shows a block diagram of the system with the final control scheme in the discretized form. For simplicity the anti-windup is not illustrated in the block diagram. The forward estimator simply takes the derivative of the positions to obtain the velocities. The output filter is a vector of first order low-pass filters with equal cut-off frequencies 100 times higher than the fastest of the system's respective bandwidths.
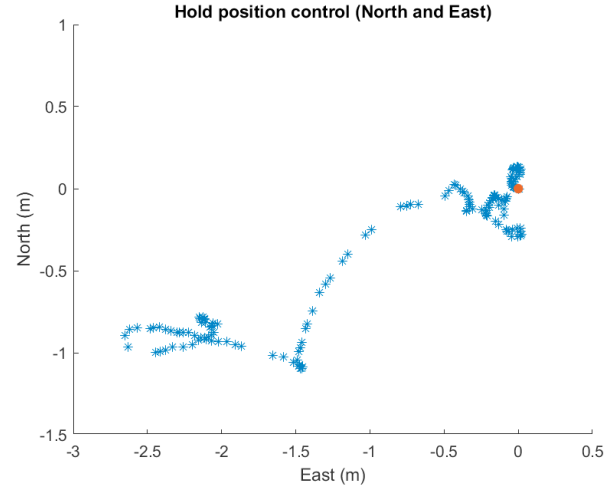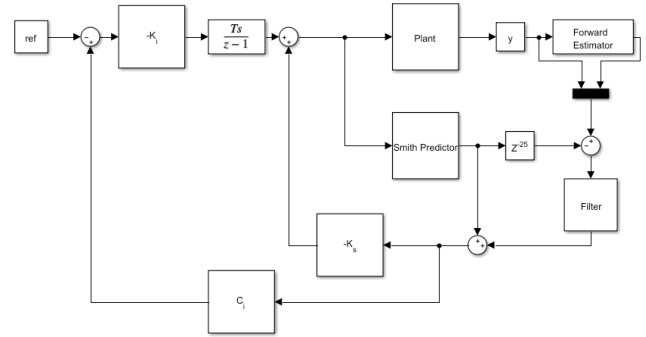

Fig. 9. The entire discretized closed-loop control structure with LQRI and Smith Predictor.

5. RESULTS

The closed-loop results are based on experimental results in a water pool. The first experiment is focusing on keeping a two-dimensional position in the north and east directions; see figure 10 which plots the two-dimensional motion during a 10 second test. It is clear that the ROV drifts and that the controller does not operate as intended. The controller gains are now reduced to observe if it improves the stabilization; see figure 11 which plots the two-dimensional motion during a 10 second test. As it still drifts it is concluded that the Smith predictor does not work well for handling the time delay on the output, probably due to the time delay being time variant. Lastly, a test is carried out where only the yaw and heave is controlled as they are not effected by the UAPS' time delay. If these motions are stable without further tuning it is clear that it is verified that the Smith predictor caused the problems for the control scheme. This test is seen in figure 12. It is clear that, although there are more fluctuations present for both heave and yaw in the experiments than in simulations, both output drifts. By reducing the integral gains the fluctuations are expected to be reduced, however, by now it is clear that the developed
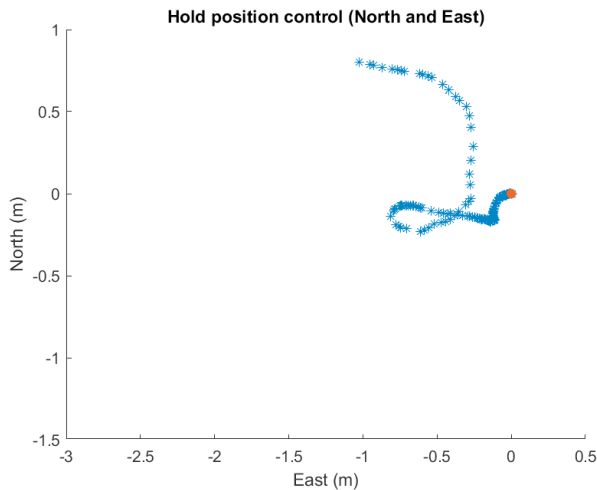
Fig. 11. Result for steady position controller with the final tune of the controller, the red dot is the initial position.
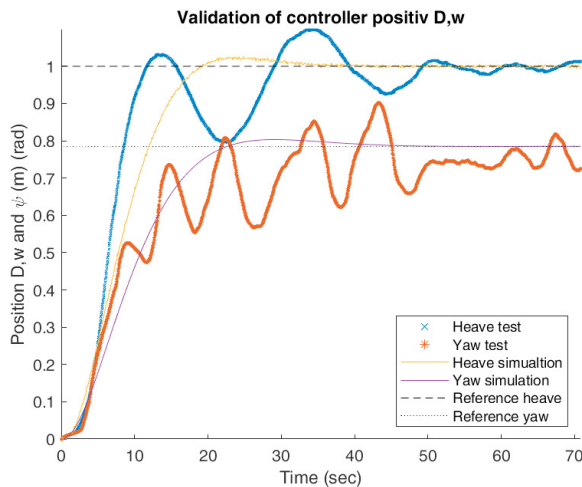

Fig. 12. Result comparison of the test and the simulation of the controller for yaw and heave

LQRI controller operates better than the UAPS controller.

6. CONCLUSION

This study examines the modeling, identification and control of a BlueROV2 using an UAPS underwater position transmitter. The model is shown to fit the obtained data acceptably but with some deviations from reality. The developed LQRI controller with a Smith predictor did not stabilize the ROV in a two-dimensional space, probably because the Smith predictor not properly eliminating the negative effect of the UAPS time delay. When controlling the ROV using alternative heave and yaw transmitters the control scheme operates better. In future work an online identification of the time delay will be used to catch the potential time-variant features. At this stage it is uncertain how fast the time delay changes with respect to time and, thus, the cause of the communication delay needs to be examined further.

REFERENCES

Arnesen, B.O., Lekkas, A.M., and Schjoelberg, I. (2017). 3d path following and tracking for an inspection class rov. *ASME 36th International Conference on Ocean, Offshore and Arctic Engineering*, 7a(OMAE2017-61170), V07AT06A019.

Brun, L. (2014). ROV/AUV Trends: Market and Technology. *DOI: 10.13140/RG.2.1.4062.5686*.

Cengel, Y. (2012). *Fundamentals of Thermal-Fluid sciences*. McGraw-Hill. ISBN-13: 978-0071325110.

Fossen, T.I. (1994). *Guidance and Control of Ocean Vehicles*. Wiley. ISBN-13: 978-0471941132.

Fossen, T.I. (2011). *Handbook of Marine Craft Hydrodynamics and Motion Control*. Wiley. ISBN: 978-1-119-99149-6.

Joaqun Aparicio, A.J. and lvarez, F.J. (2016). Characterization of an underwater positioning system based on gps surface nodes and encoded acoustic signals. *IEEE Transactions on Instrumentation and Measurement*. URL https://ieeexplore.ieee.org/stamp/stamp.jsp?tp=&arnumber=7469873.

Mai, C., Pedersen, S., Hansen, L., Jepsen, K.L., and Yang, Z. (2016). Subsea infrastructure inspection: A review study. In *2016 IEEE International Conference on Underwater System Technology: Theory and Applications (USYS)*, 71–76.

Mai, C., Pedersen, S., Hansen, L., Jepsen, K.L., and Yang, Z. (2017). Modeling and Control of Industrial ROV's for Semi-Autonomous Subsea Maintenance Services. *IFAC Congress*.

Marine Technology Society (2017). ROV Applications - What ROVs can do. *Online*. URL http://www.rov.org/rov_applications.cfm.

Pedersen, S., Enevoldsen, T.T., and Einarsson, E.M. (2018). Model comparison of a videoray pro 4 underwater rov. *IEEE/ASME International Conference on Advanced Intelligent Mechatronics (AIM)*. doi:10.1109/AIM.2018.8452445.

Reid, A. (2013). ROV Market Prospects. *Subsea UK, Aberdeen*. URL http://www.subseauk.com/documents/presentations/ssuk%20-%20rov%20event%20-%20sep%202013%20%5Bweb%5D.pdf.

Schjølberg, I. and Utne, I.B. (2015). Towards autonomy in rov operations. *IFAC-PapersOnLine*, 48(2), 183 – 188.

Tena, I. (2011). Automating ROV Operations in aid of the Oil & Gas Offshore Industry. *SeeByte Whitepaper*.

Wang, W. and Clark, C.M. (2006). Modeling and Simulation of the VideoRay Pro III Underwater Vehicle. *IEEE OCEANS 2006*.

Wynn, R.B., Huvenne, V.A., Bas, T.P.L., Murton, B.J., Connelly, D.P., Bett, B.J., Ruhl, H.A., Morris, K.J., Peakall, J., Parsons, D.R., Sumner, E.J., Darby, S.E., Dorrell, R.M., and Hunt, J.E. (2014). Autonomous Underwater Vehicles (AUVs): Their past, present and future contributions to the advancement of marine geoscience. *Marine Geology*, 352, 451 – 468.